Since January 2020 Elsevier has created a COVID-19 resource centre with free information in English and Mandarin on the novel coronavirus COVID-19. The COVID-19 resource centre is hosted on Elsevier Connect, the company's public news and information website.

Journal of Hazardous Materials 280 (2014) 356–363

Contents lists available at ScienceDirect

Journal of Hazardous Materials

journal homepage: www.elsevier.com/locate/jhazmat

Fabrication of an anti-viral air filter with SiO_2–Ag nanoparticles and performance evaluation in a continuous airflow condition

Yun Haeng Joe [a], Kyoungja Woo [b], Jungho Hwang [a,*]

[a] School of Mechanical Engineering, Yonsei University, Seoul 120-749, Republic of Korea
[b] Molecular Recognition Research Center, Korea Institute of Science and Technology, Cheongryang, Seoul 130-650, Republic of Korea

HIGHLIGHTS

- SiO_2 particles surface coated with Ag particles were fabricated to coat an air filter.
- An anti-viral ability of the filter was evaluated against aerosolized virus particles.
- A mathematical approach of an anti-viral ability of the air filter was developed.
- A quality factor based on an anti-viral ability of the air filter was proposed.

GRAPHICAL ABSTRACT

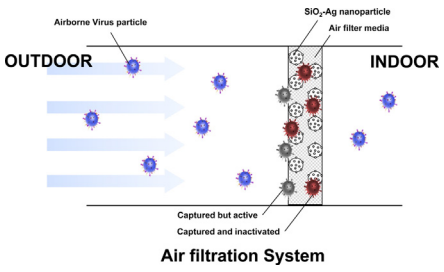

ARTICLE INFO

Article history:
Received 21 May 2014
Received in revised form 21 July 2014
Accepted 9 August 2014
Available online 19 August 2014

Keywords:
Airborne virus
Anti-viral air filter
Filter quality
SiO_2–Ag nanoparticle

ABSTRACT

In this study, SiO_2 nanoparticles surface coated with Ag nanoparticles (SA particles) were fabricated to coat a medium air filter. The pressure drop, filtration efficiency, and anti-viral ability of the filter were evaluated against aerosolized bacteriophage MS2 in a continuous air flow condition. A mathematical approach was developed to measure the anti-viral ability of the filter with various virus deposition times. Moreover, two quality factors based on the anti-viral ability of the filter, and a traditional quality factor based on filtration efficiency, were calculated. The filtration efficiency and pressure drop increased with decreasing media velocity and with increasing SA particle coating level. The anti-viral efficiency also increased with increasing SA particle coating level, and decreased by with increasing virus deposition time. Consequently, SA particle coating on a filter does not have significant effects on filtration quality, and there is an optimal coating level to produce the highest anti-viral quality.

1. Introduction

In recent years, airborne microorganisms such as viruses, bacteria, and fungi have become factors of interest for indoor air quality because they can cause acute or chronic disease, which may be infectious, allergenic, or toxigenic [1–5]. Viral infection outbreak events caused by fatal viruses, such as highly pathogenic avian influenza virus (HPAIV), severe acute respiratory syndrome (SARS) coronavirus, and novel swine-origin influenza A (H1N1) have increased concerns over viral infection.

The viruses, which are nanometers in size, can persist in small droplets, and remain suspended in the air long enough to be dispersed [6]. Previous studies reported that viruses can exist in the air of hospital rooms [7,8] and also in human breath [9,10]. Moreover, large scale outbreaks of SARS were caused via airborne exposure routes [11,12]. An airborne infection which occurs by transportation of virus-laden aerosols plays an important role in disease

* Corresponding author at: School of Mechanical Engineering, Yonsei University, 134 Shinchon-dong, Seodaemun-gu, Seoul 120-749, Republic of Korea.
Tel.: +82 2 2123 2821; fax: +82 2 312 2821.
E-mail addresses: kazamajo@nate.com (Y.H. Joe), kjwoo@kist.re.kr (K. Woo), hwangjh@yonsei.ac.kr (J. Hwang).

http://dx.doi.org/10.1016/j.jhazmat.2014.08.013
0304-3894/

dispersion, thus, development of efficient air control technology is important in combating inhalation-related diseases. Antimicrobial agent treatment is a possible solution to prevent airborne infection. Therefore, the synthesis of various antimicrobial agents and their applications for air purification have been studied.

Ag nanoparticles have been widely used as an antimicrobial agent, and synthesized by various methods. Ion reduction is one of the methods for synthesis of Ag nanoparticles in aqueous media. The ion reduction method is used in the presence of stabilizer [13], especially, reducing Ag^+ ions on the surface of support materials is recommended to provide stability against aggregation [14–16]. Numerous researchers have used several different support materials such as polymers [17–19], inorganic layers [20–22], and the materials at which the surface is functionalized [14,23–27]. In addition to the ion reduction method, a spark discharge system is suitable for synthesizing in both gas and liquid media [28,29].

It is known that anti-viral agents act directly by lysing viral membranes on contact or by binding to virus coat proteins. The mechanism of action of Ag nanoparticles as an antiviral agent has been studied against several enveloped viruses. It is suggested that nanoparticles bind with a viral envelope glycoprotein and inhibit the virus by binding to the disulfide bond regions of the cluster of differentiation 4 (CD4) binding domain within the human immunodeficiency virus 1 (HIV-1) viral envelope glycoprotein gp120 [30,31]. Moreover, it is reported that silver nanoparticles have high binding affinity for the hepatitis B virus (HBV) DNA and extracellular virions with different sized Ag nanoparticles, and can inhibit the production of HBV RNA and extracellular virions [32]. It is generally understood that Ag ions and Ag nanoparticles inactivate viruses by denaturing enzymes by reactions with sulfhydra, amino, carboxyl, phosphate, and imidazole groups [33–37].

Several research groups studied the inactivation of airborne viruses via various technologies. Kettleson et al. [38] used an electrostatic precipitator (ESP) for capturing and inactivating aerosolized bacteriophages T3 and MS2. Grinshpun et al. [39] investigated inactivation of aerosolized bacteriophage MS2 in a continuous air flow chamber with axial heating for periods of 0.1–1 s. Pyankov et al. [40] used sprayed tea tree and eucalyptus oils for inactivating influenza virus A stain NWS/G70C (H11N9). However, to our knowledge, no research on the inactivation of airborne viruses by Ag nanoparticles has been released to the public.

In a previous study, magnetic silica hybrid particles (0.5–0.7 μm in diameter) decorated with Ag nanoparticles were synthesized, and their antimicrobial ability against *Escherichia coli* and bacteriophage MS2 virus was evaluated in liquid media [26]. A following study presented a large scale fabrication of monodisperse silica hybrid particles (without magnetic core) decorated with Ag nanoparticles and their prompt antibacterial activity against both Gram-negative and Gram-positive bacteria on air filtration [27]. In those studies, the silica hybrid particles, whether they contained a magnetic Fe_3O_4 core or not, were functionalized with aminopropyl (AP) groups and the AP groups were used as a dispersive supporter for aggregation control in an aqueous solution and also, as a post to decorate Ag nanoparticles. Oxidation of the decorated Ag nanoparticles was negligibly minimal and their integral hybrid structure was conserved even after 8 months, as far as their concentration had been kept higher than 1.3% in aqueous media. Moreover, surface-oxidized Ag nanoparticles on silica still exhibited a promising antibacterial activity both in water and air [27].

In this study, the SiO_2–Ag nanoparticles (hereafter called SA particles) were synthesized by the procedure reported in Ref. [27] except with a magnetic Fe_3O_4 cluster. Then, we applied particles for fabricating an anti-viral air filter. The pressure drop, filtration efficiency, and anti-viral ability of the fabricated filter were evaluated against aerosolized bacteriophage MS2.

2. Materials and methods

2.1. Synthesis of nanoparticles

SA particles were prepared by four steps. (1) Synthesis of silver seeds. (2) Synthesis of silica spheres. (3) Functionalization of silica surface with AP group. (4) Attachment of silver seeds on the functionalized silica sphere and size growth of the seeds. In order to synthesize silver seeds, NaOH (Showa, 93.0%) solution, Tetrakis (hydroxymethyl phosphonium chloride) (THPC, Sigma–Aldrich, 80% solution in water), and $AgNO_3$ (Sigma–Aldrich, 99.8–100.5%) solution were used. THPC is known as a formaldehyde-substituted phosphine of formula $P(CH_2OH)_4Cl$ and a safe and convenient reducing agent for Au^{3+} in water as it generates active reducing agent, formaldehyde, and hydrolyzes to $O_2P(CH_2OH)_3$ as shown in reactions (1) and (2) [41]. The generated $O_2P(CH_2OH)_3$ is considered to protect Au seeds from aggregation. Similarly, the reduction of Ag^+ by formaldehyde is well-known as in reactions (3) and (4) [42]. Therefore, the same chemistry for the synthesis and protection of Ag seeds was applied in this paper.

$$P(CH_2OH)_4{}^+ + OH^- \rightarrow P(CH_2OH)_3 + CH_2O + H_2O \quad (1)$$

$$P(CH_2OH)_3 + 2H_2O \rightarrow O_2P(CH_2OH)_3 + 2H_2 \quad (2)$$

$$2Ag^+ + CH_2O + 3OH^- \rightarrow 2Ag + HCOO^- + 2H_2O \quad (3)$$

$$2Ag^+ + 2CH_2O + 2OH^- \rightarrow 2Ag + 2HCOOH + H_2 \quad (4)$$

For the synthesis of silica spheres (~400 nm), OH^--catalyzed hydrolysis and condensation reaction of tetraethylorthosilicate (TEOS, Sigma–Aldrich) precursors were applied as follows [43].

$$Si(OCH_2CH_3)_4 + 4H_2O \rightarrow Si(OH)_4 + 4CH_3CH_2OH \quad (5)$$

$$nSi(OH)_4 \rightarrow nSiO_2 + 2nH_2O \quad (6)$$

After synthesis of silica spheres, OH^--catalyzed hydrolysis and condensation reaction of 3-aminopropyltri(methoxy)silane precursors were applied for AP functionalization of silica spheres, as in reactions (7) and (8).

$$Si(OCH_3)_3(CH_2CH_2CH_2NH_2) + 3H_2O \rightarrow Si(OH)_3(CH_2CH_2CH_2NH_2) + 3CH_3OH \quad (7)$$

$$nSi(OH)_3(CH_2CH_2CH_2NH_2) + nOH^- \rightarrow nSiO_2(CH_2CH_2CH_2NH_2) + 2nH_2O \quad (8)$$

The functionalized silica spheres and Ag seeds solutions were mixed, and gently swirled every 30 min. For the growth of Ag seeds into ~30 nm-sized Ag nanoparticles on a silica sphere, reactions (3) and (4) are too fast to control due to high standard redox potential (+0.80 V). Reduction of $[Ag(NH_3)_2]^+$ complexes prepared in NH_4OH solution was controllable due to the decreased reduction potential (+0.38 V) [44], which means decreased reduction rate, and generated nicely grown Ag nanoparticles on a silica particle. Then, 50 mL of the solution was used for coating after being centrifuged 3 times (4000 rpm, 10 min). The detail procedure of synthesis method was introduced in Ref. [27].

2.2. Fabrication of an anti-viral air filter

In this study, glass fiber medium filters which have 0.04 ± 0.005 cm of thickness, 0.0095 ± 0.0003 of solidity, and 1.08 ± 0.36 μm of fiber diameter were chosen to fabricate anti-viral air filters. The method of fabricating an anti-viral air filter

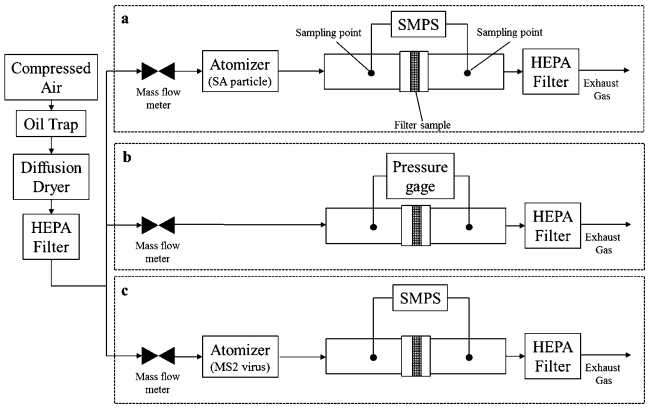

Fig. 1. Experimental setup for (a) Fabrication. (b) Pressure drop test, and (c) filtration test.

is shown in Fig. 1a. After 2 lpm of compressed air which was controlled by a mass flow meter (MFM, 4140, TSI Inc., USA) passed through a clean air supply system consisting of an oil-trap, diffusion dryer, and high efficiency particulate air (HEPA) filter, the air entered a Collison-type atomizer (9302, TSI Inc., USA) which was filled with 50 mL of SA particle solution. The aerosolized nanoparticles were carried in a flow and coated on the glass fiber medium air filter. The particle concentrations upstream (C_{in}) and downstream (C_{out}) from the filter sample were measured by a scanning mobility particle sizer (SMPS, TSI Inc., USA) which consisted of a classifier controller (3080, TSI Inc., USA), a differential mobility analyzer (DMA, 3081, TSI Inc., USA), a condensation particle counter (CPC, 3022A, TSI Inc., USA), and an aerosol charge neutralizer (Soft X-ray charger 4530, HCT Co., Ltd., Korea). The sampling air flow rate of the SMPS was 0.3 lpm. The coating areal density (ρ_{areal}) of the air filter was calculated by the following equation,

$$\rho_{areal} = \frac{Qt(C_{in} - C_{out})}{A} \quad (9)$$

where Q is the flow rate, t is the coating time, and A is the area of the filter sample (4 cm × 4 cm). The evolution of the SA particle dendrites on the filter fibers was observed using an environmental scanning electron microscope (ESEM; XL30-ESEM, FEI, USA).

2.3. Preparation of microorganism solutions

The bacteriophage MS2 virus (ATCC 15597-B1), and *Escherichia coli* strain C3000 (ATTCC 15597) were used as test virus and host bacteria, respectively. In order to restore the bacterial cells from their freeze-dried state, 10 mL of tryptic soy broth (TSB) was injected into the freeze-dried cells and the mixture was shaken and incubated for 24 h at 37 °C. Then, 0.1 mL of incubated bacterial solution was injected into the 10 mL of TSB, and the mixture was used as a host bacterial solution after additional shaking incubation for 6 h at 37 °C.

1 mL of TSB was injected into the freeze-dried MS2 virus. Then, 0.1 mL of the solution was mixed with 0.3 mL of host bacterial solution and 29 mL of soft tryptic soy agar (TSA) containing 8 g/L of agar. The melted TSA was maintained at 48 °C till ready to pour. The mixture was poured onto a petri dish and allowed to dry. The hardened agar plate was incubated at 37 °C overnight, and then the surface of the agar was scraped off with 10 mL of phosphate buffer solution (PBS) whose pH was maintained at 7.0. The solution was mixed with 10 mL of chloroform ($CHCl_3$), and centrifuged for 20 min at 5000 × g, and the supernatant was conserved. 0.1 mL of the supernatant was diluted with 50 mL DI water, and the solution was used as a virus solution.

2.4. Pressure drop and filtration test

The pressure drop across the fabricated air filter was measured using a digital pressure measuring device (Model 435-1, Testo, Germany) with various coating areal densities and with various media velocities of clean air in the range from 0.025 to 0.1 m/s (Fig. 1b). The measured pressure drop data were verified with theoretical predictions carried out using equation [45].

$$\Delta P = \frac{4\mu\alpha Lu(1 + 1.996K_n)}{0.25d_f^2\left\{-0.5\ln\alpha - 0.75 + \alpha - (\alpha^2/4) + 1.996K_n(-0.5\ln\alpha - 0.25 + (\alpha^2/4))\right\}} \quad (10)$$

where α is the filter solidity (dimensionless), L is the depth of the filter (m), μ is the dynamic viscosity of air (Pa s), d_f is the diameter of the glass fiber (m), and K_n is the Knudsen number (dimensionless). The media velocity (u, m/s) is defined as $Q/A(1-\alpha)$. The solidity of the fabricated filter was calculated with the following equation,

$$\alpha = \alpha' + \alpha_{particle} \quad (11)$$

where α' is the filter solidity of the pristine filter, which can be calculated by using $\alpha' = M_f/(\rho_f AL)$, where M_f is the filter mass, and ρ_f is the glass fiber density. $\alpha_{particle}$ is the solidity added by the coated SA particles and is calculated by using the equation, $\alpha_{particle} = V_p\rho_{areal}/AL$, where V_p is the volume of a SA particle.

The experimental setup to evaluate filtration efficiency of the fabricated filter is shown in Fig. 1c. The virus solution was aerosolized by an atomizer, and the aerosols entered a test duct in which a fabricated filter was installed. Two sampling probes were placed before and after the filter media for aerosol sampling. The aerosolized virus concentrations upstream (C_{in}) and downstream (C_{down}) from the filter were measured by a scanning mobility particle sizer (SMPS). The filtration efficiency (η_{filt}) of the filter was calculated as follows,

$$\eta_{filt} = 1 - \frac{C_{in}}{C_{out}} \quad (12)$$

2.5. Anti-viral test

Virus particles were aerosolized by an atomizer, and deposited onto each filter sample for 30 min. Each filter was put into 10 mL of DI water, and was under sonication for 10 min with a batch-type sonicator (KMC1300 V, Vision scientific, Korea) to detach the deposited virus particles from the filter. Then, the number of virus particles, which were infectious to *E. coli*, in the DI water was evaluated with the single agar layer method [46]: 0.1 mL of the solution was mixed with 0.3 mL of host bacterial solution and 29 mL of soft TSA which was maintained at 48 °C. Then the mixture was poured into the petri-dish. After overnight incubation at 37 °C, the number of plaques was counted. Finally, the overall anti-viral efficiency was calculated using the following equation,

$$\bar{\eta}_{antiviral} = 1 - \frac{PFU_i}{PFU_0} \quad (13)$$

where *PFU* is the concentration of virus particles (PFU/m^3, plaque forming unit), and subscripts i and 0 represent the SA particle coated filter with various coating areal densities and a pristine filter, respectively.

In order to evaluate detachment efficiency of the sonication, η_{detach}, an additional experiment was performed. A drop of virus solution was dropped onto the pristine filter, and allowed to dry. The filter was put into 10 mL of DI water and sonicated for 10 min. Then, the number of virus particles in the drop of virus solution and also that in the used DI water were evaluated with the single

agar layer method. The detachment efficiency was calculated by the following equation,

$$\eta_{\text{detach}} = 1 - \frac{PFU_{\text{DW}} \times V_{\text{DW}}}{PFU_{\text{drop}} \times V_{\text{drop}}} \quad (14)$$

where V is the volume of the liquid, and subscripts DW and drop represent the used DI water and a drop of virus solution, respectively.

During the sonication process, SA particles which are detached from the filter can cause anti-viral action in the water media. In addition, Ag^+ ions which are diffused from the SA particles to the water media can result in additional antiviral action. Thus, the following additional experiments were carried out to evaluate effects of Ag^+ ions and detached SA particles on anti-viral action. A virus-free SA particle-coated filter which had 1.2×10^9 number of particles (#) per unit filter surface area (cm^2) of coating areal density (maximum coating areal density in this study) was put into 10 mL of DI water, and was under sonication for 10 min. After sonication, the filter was separated from the DI water, where Ag^+ ions and SA particles might be dissolved. Then, aerosolized virus particles were deposited on the pristine filter for 30 min. The virus-contaminated filter was put into the DI water used in the previous step, and was under sonication for 10 min, so that virus particles could be contained in the DI water. The number of infectious virus particles in the solution was evaluated with the single agar layer method, and the anti-viral efficiency due to both the Ag^+ ions and detached SA particles was calculated using Eq. (13).

3. Results and discussion

3.1. Fabrication of anti-viral air filter

The size distribution of aerosolized SA particles measured upstream of the filter with the SMPS is shown in Fig. 2. The mode diameter of the SA particles was about 430 nm. The geometric standard derivation and total number concentration were 2.30 and 1.8×10^5 number of particles (#) per unit air volume (cm^3), respectively. It is observed that residue particles smaller than 100 nm still remained in the solution even after three rounds of centrifuging, but their amount was negligible. Fig. 2 also shows the size distribution of the SA particles measured downstream of the filter after the coating process. The difference between the upstream concentration and the downstream concentration was continuously monitored during the process. Fig. 3 shows an ESEM image of

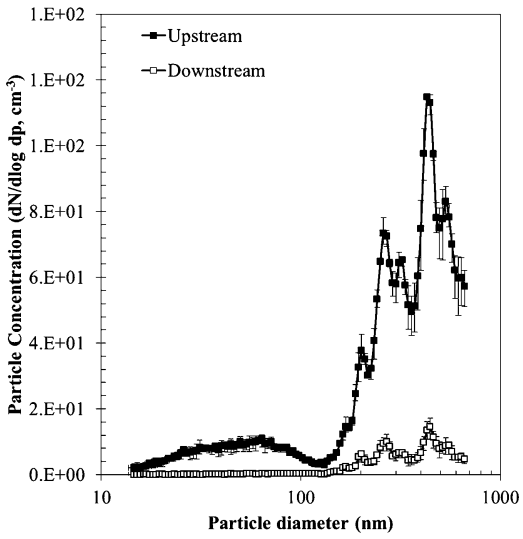

Fig. 2. SA particles concentrations upstream and downstream of the filter.

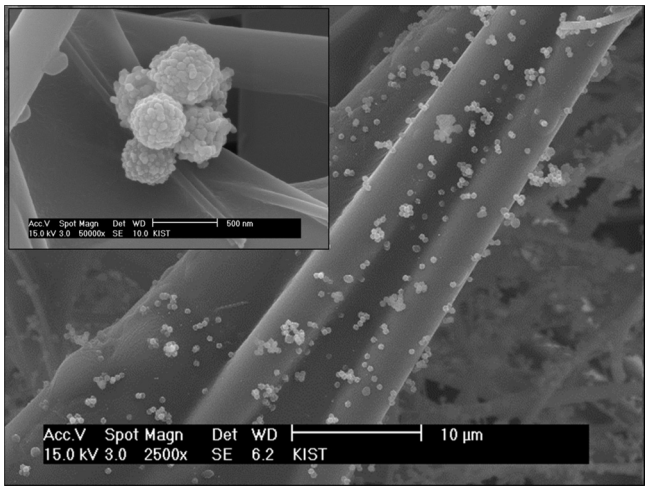

Fig. 3. ESEM image of SA particle coated air filter.

the fabricated filter. It is seen that SA particles were well distributed and coated on the glass fiber. The size of the SA particles was about 400–450 nm, which matched the SMPS data. The SA particle coated filters were fabricated with various coating areal densities from 2.0×10^7 to 1.2×10^9 #/cm^2.

A pressure drop test was carried out with the fabricated filters. For each filter, pressure drops were measured with various coating areal densities and media velocities. Fig. 4 shows that for any media velocity, the pressure drop increased as the coating areal density increased. Similarly, the pressure drop increased as the media velocity increased, for a given coating areal density. The filter with an areal density of 1.2×10^9 #/cm^2 had solidity of about 0.01, while the solidity of the pristine filter (α') was 0.009. The increment of solidity ($\alpha_{\text{particle}} = 0.001$) was enough to disturb the flow inside the filter and change the pressure drop. Theoretical values predicted by Eq. (10) were consistent with the experimental tendency. Moreover, an experiment was carried out using 0.5 m/s of clean air to investigate whether coated SA particles could be detached from the filter. The concentration downstream from the fabricated filter

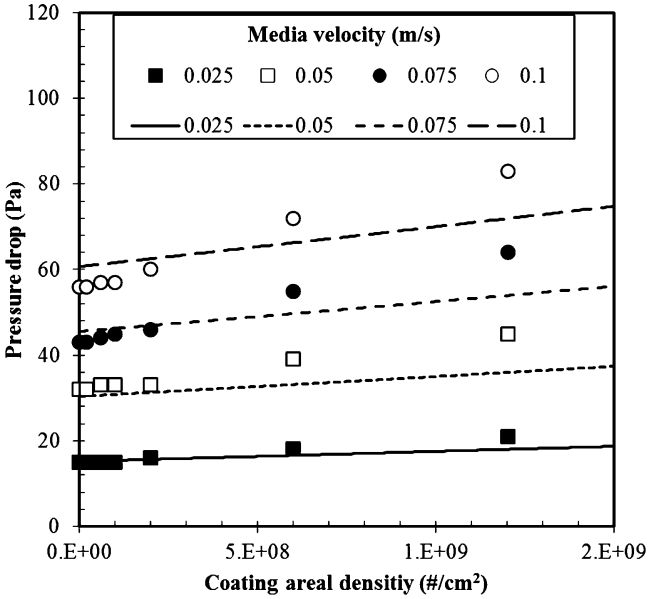

Fig. 4. Pressure drop of fabricated filter; symbol: experimental data, line: calculated by Eq. (10).

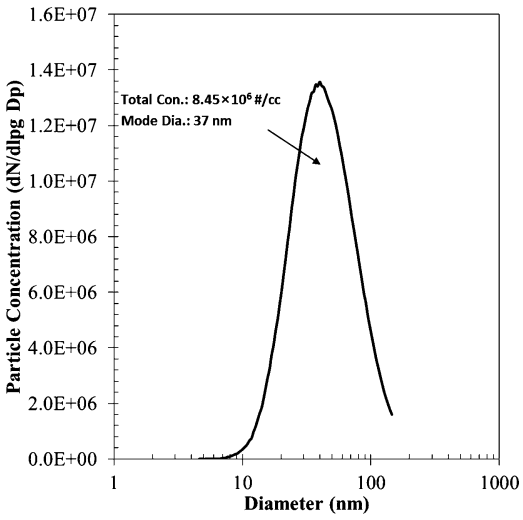

Fig. 5. Size distribution of aerosolized MS2 particles.

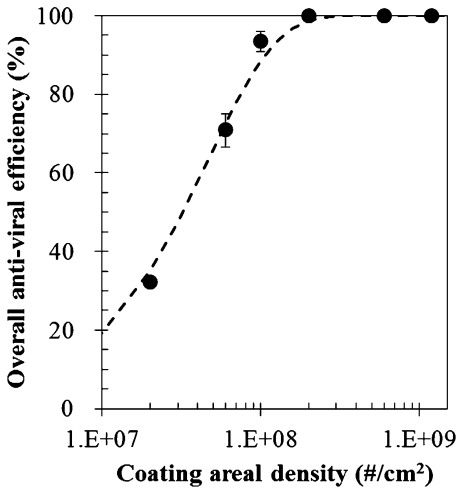

Fig. 7. Overall anti-viral efficiency of the fabricated filter with various coating areal density.

was measured by the CPC, and the results show that no SA particles were detached from any fabricated filter samples.

3.2. Filtration of aerosolized MS2

The size distribution of aerosolized MS2 is shown in Fig. 5. The mode diameter of the aerosolized virus particles was 37 nm. The geometric standard derivation and number concentration were 1.7 and 8.45×10^6 #/cc, respectively. Filtration efficiencies of fabricated air filters for various coating areal densities and media velocities are shown in Fig. 6. The filtration efficiency increased with decreasing media velocity for a given coating areal density. It is well known that the filtration mechanism for nanoparticles at the tens-of-nanometer scale is dominated by diffusional motion of the particles. It is well known that the filtration efficiency due to Brownian diffusion increases with decreasing media velocity for a given particle size [47]. The experimental results shown in Fig. 6 follow this tendency. Moreover, Fig. 6 shows that the filtration efficiency increased with increasing coating areal density for a given media velocity. In previous research, the filtration efficiency of a particle-loaded filter was suggested as follows [48],

$$\eta_{filt} = 1 - P_0 exp[-\beta \rho_{areal}] \quad (15)$$

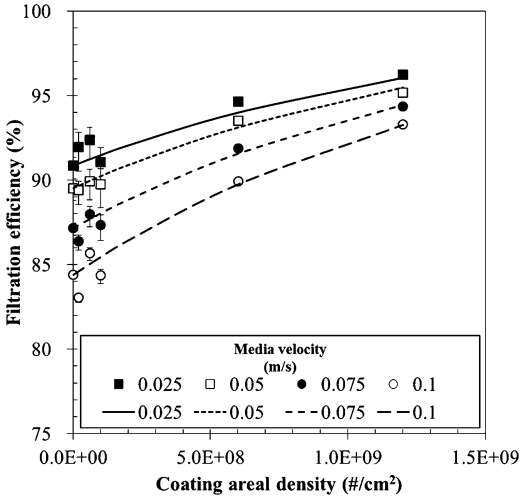

Fig. 6. Filtration efficiency of the fabricated filter with various coating areal densities and media velocities; symbol: experimental data, line: calculated by Eq. (15).

where P_0 is the penetration of the particle unloaded filter, depending on the media velocity. β is a constant representing filter performance, which depends on the filter material. The experimental results were well predicted by Eq. (15) when β was set as 7.0×10^{-10} cm^2.

3.3. Anti-viral effect

The effect of sonication on the number of detached virus particles was tested (detachment test). From repeated measurements of the detachment test, the detachment efficiency, η_{detach}, was obtained as 0.3 ± 0.03, which means that 30% of captured virus particles were detached and re-suspended in the DI water. Fig. 7 shows the overall anti-viral efficiency of the fabricated filter with various coating areal densities. The efficiency exponentially increased as the coating areal density increased, and most virus particles (99.9%) lost their infectiousness when the coating areal density was higher than 2.0×10^8 #/cm^2.

It was found that the anti-viral action with Ag ions and SA particles diffused and detached from the filter ($\rho_{areal} = 1.2 \times 10^9$ #/cm^2), respectively, was 1.6 ± 3.8%. Therefore, it can be concluded that the anti-viral action of SA particles against MS2 was mostly performed when MS2 particles contacted the SA particles on the filter in an air media.

Even though the overall anti-viral efficiency can be used to compare anti-viral abilities between various SA particle-coated air filters, there are two issues which should be addressed. The first issue is about the ratio of the number of virus particles deposited on the filter to the SA particles in the filter. As shown in Fig. 7, the overall anti-viral efficiency was strongly influenced by the amount of SA particles coated in a filter. Note that each data point was determined with Eq. (13) and plaque counting was performed for a filter after the filter was continuously deposited by the aerosolized virus particles for 30 min. However, for virus deposition times other than 30 min, different antiviral efficiencies would be obtained. If the deposition time increases, the ratio of the number of virus particles to SA particles will increase, implying that the amount of SA particles would not be enough for antiviral action against the virus particles. The second issue is about the fact that the filtration efficiency increased with the coating areal density. As shown in Fig. 6, the filtration efficiency was a function of coating areal density, thus, the amount of deposited virus particles increased with coating areal density for a given virus deposition time.

In order to consider these two issues as well as the results of Fig. 7, the time dependent anti-viral efficiency, $\eta_{antiviral}(t)$, can be

expressed with a modified exponential rise to max equation, as follows,

$$\eta_{\text{antiviral}}(t) = 1 - exp\left[-\alpha \frac{\rho_{\text{areal}}}{\dot{N}_{\text{depo}} t}\right] \tag{16}$$

where α is a dimensionless value and t is the virus deposition time. $\dot{N}_{\text{depo}}$ is the flux of deposited virus particles (PFU/cm^2/min) which is determined by the filtration efficiency as follows,

$$\dot{N}_{\text{depo}} = \eta_{\text{filt}} \dot{N}_{\text{in}} \tag{17}$$

where $\dot{N}_{\text{in}}$ is the flux of entering virus particles (PFU/cm^2/min). The unknown value α can be a function of the characteristics of the filter and coated anti-viral agent, species of virus particles, and deposition of dust particles which can interrupt the contact between virus particles and the anti-viral agent. In this study, all of the experiments were performed in clean air (no dust effect) and only one virus species was considered. Thus, α was assumed to be constant for simplification.

Using Eq. (16), the number of surviving virus particles per unit area (N_{surv}, PFU/cm^2) can be calculated as follows,

$$\begin{aligned} N_{\text{surv}} &= \int_0^{\tau} (1 - \eta_{\text{antiviral}}(t)) \dot{N}_{\text{depo}} dt \\ &= \dot{N}_{\text{depo}} \tau \exp\left[-\alpha \frac{\rho_{\text{areal}}}{\dot{N}_{\text{depo}} \tau}\right] + \alpha \rho_{\text{areal}} Ei\left[-\alpha \frac{\rho_{\text{areal}}}{\dot{N}_{\text{depo}} \tau}\right] \end{aligned} \tag{18}$$

where τ is the operating time (i.e., virus deposition time), and a function $Ei(z)$ is the exponential integral function defined as

$$Ei(z) = -\int_{-z}^{\infty} \frac{e^{-t}}{t} dt \tag{19}$$

Using the experimental results of PFU_i and PFU_0, the values of $\dot{N}_{\text{in}}$, and N_{surv} were calculated as follows,

$$\dot{N}_{\text{in}} = \frac{\eta_{\text{filt}}}{\eta_{\text{detach}} \eta_{\text{filt},0}} \frac{l \times \text{PFU}_0}{A\tau} \tag{20}$$

$$N_{\text{surv}} = \frac{1}{\eta_{\text{detach}}} \frac{l \times \text{PFU}_{\text{i}}}{A} \tag{21}$$

where $\eta_{\text{filt},0}$ is the filtration efficiency of the pristine air filter, and l is the volume of the DI water containing virus particles detached from the filter (10 mL in this study). The values of N_{surv} theoretically calculated by Eq. (18) rapidly decreased with increasing coating areal density and were well matched with N_{surv} values determined by Eq. (21) with experimental data, when the dimensionless constant, α, was 3.15×10^{-5} and the virus deposition time, τ, was 30 min (Fig. 8a). Consequently, the time-dependent anti-viral efficiencies were calculated by substituting the value of α into Eq. (16) for various coating areal densities. The values of η_{filt} determined by Eq. (15) were also used. Fig. 8b shows that $\eta_{\text{antiviral}}(t)$ increased with coating areal density but decreased with virus deposition time. When the coating areal density was higher than 6.0×10^8 #/cm^2, no remarkable changes were induced and the anti-viral efficiency would be sustained for a long time.

3.4. Quality factors

Generally, two parameters are used to determine the performance of a filter; (1) particle collection efficiency of a filter and (2) pressure drop across the filter. The best filter is the one that gives the highest collection efficiency with the least pressure drop. However, increasing collection efficiency necessarily accompanies increasing of pressure drop. Since pressure drop is related to energy expenditure in filtration, the quotient of the logarithm of the penetration and the pressure drop is a measure of the performance achieved against the energy expended. This quotient is called the

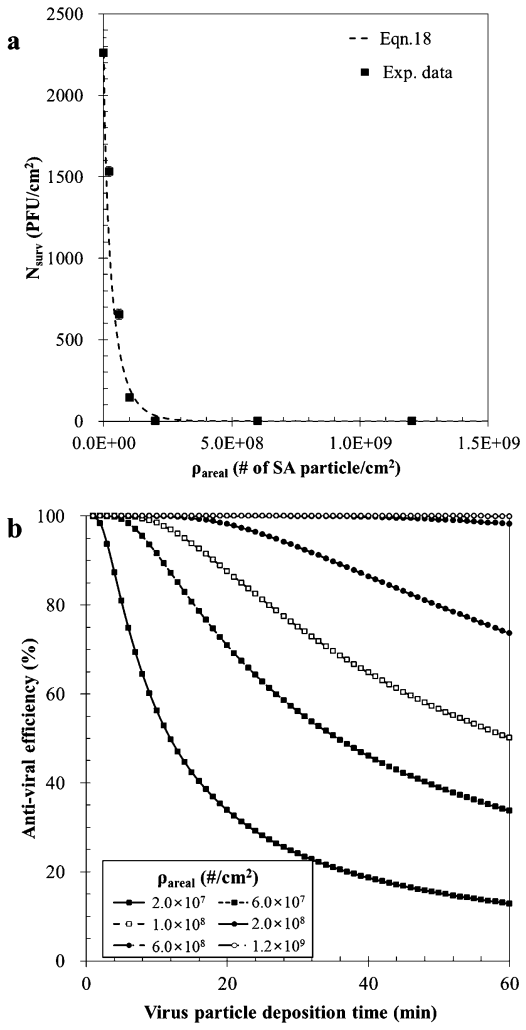

Fig. 8. Calculation results of (a) N_{surv} with various coating areal density and (b) anti-viral efficiency with various virus deposition time.

quality factor. Therefore, the quality factor is used as a useful criterion for comparing different filters of different thickness. In this study, in order to compare the performances of various anti-viral air filters, three different filter quality factors were evaluated: filtration quality factor (q_{filt}), overall anti-viral quality factor ($\bar{q}_{\text{antiviral}}$), and time-dependent anti-viral quality factor ($q_{\text{antiviral}}$), which were defined as follows,

$$q_{\text{filt}} = \frac{\ln(1/1 - \eta_{\text{filt}})}{\Delta P} \tag{22}$$

$$\bar{q}_{\text{antiviral}} = \frac{\ln(1/(1 - \bar{\eta}_{\text{antiviral}}))}{\Delta P} \tag{23}$$

$$q_{\text{antiviral}}(t) = \frac{ln(1/1 - \eta_{\text{antiviral}}(t))}{\Delta P} \tag{24}$$

The filtration quality factor (q_{filt}) decreased with increasing media velocity (Fig. 9a). However, coating areal density did not lead to significant changes in the filtration quality factor, since both filtration efficiency (η_{filt}) and pressure drop increased with increasing coating areal density. The overall anti-viral quality factor ($\bar{q}_{\text{antiviral}}$) also decreased with increasing media velocity (Fig. 9b). With increasing of coating areal density, $\bar{q}_{\text{antiviral}}$ increased for a given media velocity until the efficiency reached its maximum value (99.9%), but gradually decreased, since the pressure drop continuously increased while the anti-viral efficiency ($\bar{\eta}_{\text{antiviral}}$) was maintained at a maximum. For a given coating areal density, the

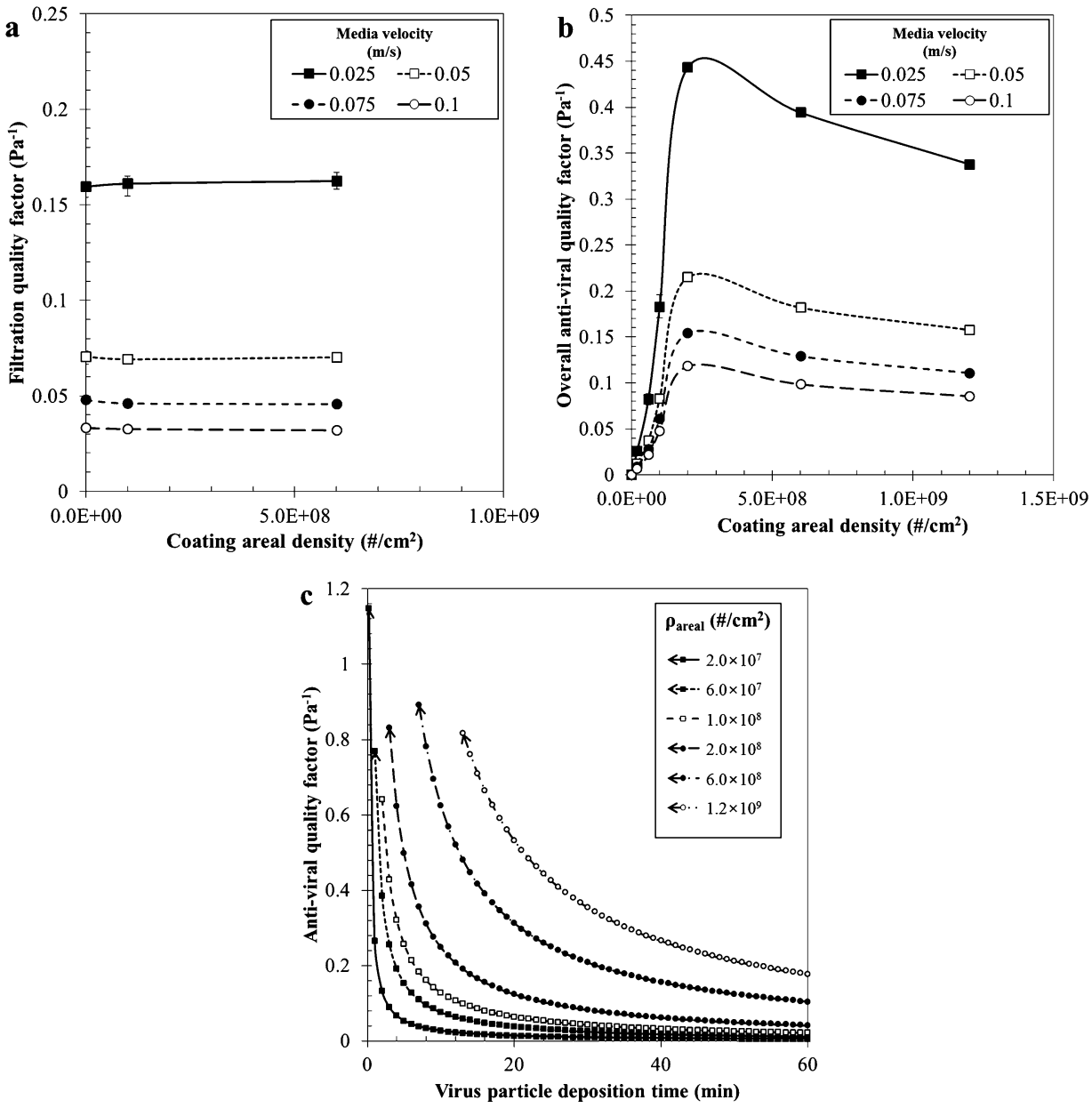

Fig. 9. Quality factors of the filter; (a) as a function of filtration efficiency, (b) as a function of overall anti-viral efficiency and (c) as a function of time dependent anti-viral efficiency @ $u = 0.05$ m/s.

time-dependent anti-viral quality factor ($q_{\text{antiviral}}(t)$) approached an infinite value due to $\eta_{\text{antiviral}}(0) \approx 1$ when the virus deposition time was close to zero and exponentially decreased with increasing virus deposition time (Fig. 9c). Moreover, with a higher coating areal density, $q_{\text{antiviral}}(t)$ gradually decreased. By comparing these quality factors, it can be concluded that coating SA particles on a filter does not lead to a significant effect on the filtration quality, and there is an optimal coating areal density to obtain the highest anti-viral quality. These factors can be used as a criterion for determining the effective coating level for an anti-viral agent.

Acknowledgements

This research was supported by Future-based Technology Development Program (Green Nano Technology Development Program) through the National Research Foundation of Korea (NRF) funded by the Ministry of Education, Science and Technology (grant number NRF-2010-0029297).

References

[1] H.J. Chao, J. Schwartz, D.K. Milton, H.A. Burge, Populations and determinants of airborne fungi in large office buildings, Environ. Health Perspect. 110 (2002) 777–782.
[2] C.E. Main, Aerobiological, ecological, and health linkages, Environ. Int. 29 (2003) 347–349.
[3] J. Douwes, P. Thome, N. Pearc, D. Heederik, Review bioaerosol health effects and exposure assessment: progress and prospects, Ann. Occup. Hyg. 47 (2003) 187–200.
[4] F. Fung, W.G. Hughson, Health effects of indoor fungal bioaerosol exposure, Appl. Occup. Environ. Hyg. 18 (2003) 535–544.
[5] T. Husman, Health effects of indoor-air microorganisms, Scand. J. Work Environ. Health 22 (1996) 5–13.
[6] W.F. Wells, Airborne Contagion and Air Hygiene, Cambridge University Press, Cambridge, 1955.

[7] F.M. Blachere, W.G. Lindsley, T.A. Pearce, S.E. Anderson, M. Fisher, R. Khakoo, Measurement of airborne influenza virus in a hospital emergency department, Clin. Infect. Dis. 48 (2009) 438–440.
[8] M.H. Sawyer, C.J. Chamberlain, Y.N. Wu, N. Aintablian, M.R. Wallace, Detection of Varicella-Zoster virus DNA in air samples from hospital rooms, J. Infect. Dis. 169 (1994) 91–94.
[9] P. Fabian, J.J. McDevitt, W.H. DeHaan, R.O. Fung, B.J. Cowling, K.H. Chan, Influenza virus in human exhaled breath: an observational study, PLoS ONE 3 (2008) e2691.
[10] S. Stelzer-Braid, B.G. Oliver, A.J. Blazey, E. Argent, T.P. Newsome, W.D. Rawlinson, Exhalation of respiratory viruses by breathing, coughing, and talking, J. Med. Virol. 81 (2009) 1674–1679.
[11] T.F. Booth, B. Kournikakis, N. Bastien, J. Ho, D. Kobasa, L. Stadnyk, Review detection of airborne sever acute respiratory syndrome (SARS) coronavirus and environmental contamination in SARS outbreak units, J. Infect. Dis. 191 (2005) 1472–1477.
[12] T.S. Yu, Y. Li, T.W. Wong, W. Tam, A.T. Chan, J.H. Lee, Evidence of airborne transmission of the severe acute respiratory syndrome virus, N. Engl. J. Med. 350 (2004) 1731–1739.
[13] N.H. Chau, L.A. Bang, N.Q. Buu, T.T.N. Dung, H.T. Ha, D.V. Quang, Some results in manufacturing of nanosilver and investigation of its application for disinfection, Adv. Nat. Sci. 9 (2008) 241–248.
[14] J.H. Park, J.K. Park, H.Y. Shin, The preparation of Ag/mesoporous silica by direct silver reduction and Ag/functionalized mesoporous silica by in situ formation of adsorbed silver, Mater. Lett. 61 (2007) 156–159.
[15] J.M. Lee, D.W. Kim, T.H. Kim, S.G. Oh, Facile route for preparation of silicasilver heterogeneous nanocomposite particles using alcohol reduction method, Mater. Lett. 61 (2007) 1558–1562.
[16] D.V. Quang, P.B. Sarawade, A. Hilonga, S.D. Park, J.K. Kim, H.T. Kim, Facile route for preparation of silver nanoparticle-coated precipitated silica, Appl. Surf. Sci. 257 (2011) 4250–4256.
[17] Y. Lv, H. Liu, Z. Wang, S. Liu, L. Hao, Y. Sang, D. Liu, J. Wang, R.I. Boughton, Silver nanoparticles-decorated porous ceramic composite for water treatment, J. Membr. Sci. 331 (2009) 50–56.
[18] P. Jain, T. Pradeep, Potential of silver nanoparticle-coated polyurethane foam as an antibacterial water filter, Biotechnol. Bioeng. 90 (2005) 59–63.
[19] M. Kríalik, A. Biffis, Catalysis by metal nanoparticles supported on functional organic polymers, J. Mol. Catal. A: Chem. 177 (2001) 113–138.
[20] L.M. Liz-Marzían, M. Giersig, P. Mulvaney, Synthesis of nanosized gold-silica core-shell particles, Langmuir 12 (1996) 4329–4335.
[21] Y. Lu, Y. Yin, Z.-Y. Li, Y. Xia, Synthesis and self-assembly of Au@SiO_2 core–shell colloids, Nano Lett. 2 (2002) 785–788.
[22] A.P. Philipse, M.P.B. van Bruggen, C. Pathmamanoharan, Magnetic silica dispersions: preparation and stability of surface-modified silca particles with a magnetic core, Langmuir 10 (1994) 92–99.
[23] H.J. Jeon, S.C. Yi, S.G. Oh, Preparation of antibacterial effects of Ag–SiO_2 thin films by sol–gel method, Biomaterials 24 (2003) 4921–4928.
[24] G. Bugla-Ploskonska, A. Leszkiewicz, B. Borak, M. Jasiorski, Z. Drulis-Kawa, A. Baszczuk, K. Maruszewski, W. Doroszkiewicz, Bactericidal properties of silica particles with silver islands located on the surface, Int. J. Antimicrob. Agents 29 (2007) 746–748.
[25] H.J. Zhang, G.H. Chen, Potent antibacterial activities of Ag/TiO_2 nanocomposite powders synthesized by a one-pot sol–gel method, Environ. Sci. Technol. 43 (2009) 2905–2910.
[26] H.H. Park, S. Park, G. Ko, K. Woo, Magnetic hybrid colloids decorated with Ag nanoparticles bite away bacteria and chemisorb viruses, J. Mater. Chem. B 1 (2013) 2701–2709.
[27] Y. Ko, Y.H. Joe, M. Seo, K. Lim, J. Hwang, K. Woo, Prompt and synergistic antibacterial activity of silver nanoparticle-decorated silica hybrid particles on air filtration, J. Mater. Chem. B (2014), http://dx.doi.org/10.1039/C4TB01068J.
[28] D.-C. Tien, K.-H. Tseng, C.-Y. Liao, T.-T. Tsung, Colloidal silver fabrication using the spark discharge system and its antimicrobial effect on *Staphylococcus aureus*, Med. Eng. Phys. 30 (2008) 948–952.
[29] Y.H. Joe, W. Ju, J.H. Park, Y.H. Yoon, J. Hwang, Correlation between the antibacterial ability of silver nanoparticle coated air filters and the dust loading, Aerosol Air Qual. Res. 13 (2013) 1009–1018.
[30] J.L. Elechiguerra, J.L. Burt, J.R. Morones, A. Camacho-Bragado, X. Gao, H.H. Lara, M.J. Yacaman, Interaction of silver nanoparticles with HIV-1, J. Nanobiotechnol. 3 (2005) 6.
[31] H.H. Lara, N.V. Ayala-Nunez, L. Ixtepan-Turrent, C. Rodriguez-Padilla, Mode of antiviral action of silver nanoparticles against HIV-1, J. Nanobiotechnol. 8 (2010) 1.
[32] L. Lu, R.W. Sun, R. Chen, C.K. Hui, C.M. Ho, J.M. Luk, G.K. Lau, C.M. Che, Silver nanoparticles inhibit hepatitis B virus replication, Antivir. Ther. 13 (2008) 253–262.
[33] C. Baker, A. Pradhan, L. Pakstis, D.J. Pochan, S.I. Shah, Synthesis and antibacterial properties of silver nanoparticles, J. Nanosci. Nanotechnol. 5 (2005) 244–249.
[34] M. Rai, A. Yadav, A. Gade, Silver nanoparticles as a new generation of antimicrobials, Biotechnol. Adv. 27 (2009) 76–83.
[35] C. Aymonier, U. Schlotterbeck, L. Antonietti, P. Zacharias, R. Thomann, J.C. Tiller, S. Mecking, Hybrids of silver nanoparticles with amphiphilic hyperbranched macromolecules exhibiting antimicrobial properties, Chem. Commun. (Camb.) (2002) 3018–3019.
[36] J.P. Ruparelia, A.K. Chatterjee, S.P. Duttagupta, S. Mukherji, Strain specificity in antimicrobial activity of silver and copper nanoparticles, Acta. Biomater. 4 (2008) 707–716.
[37] G. Borkow, J. Gabbay, Putting copper into action: copper-impregnated products with potent biocidal activities, FASEB J. 18 (2004) 1728–1730.
[38] E.M. Kettleson, B. Ramaswami, C.J.J.R. Hogan, M.H. Lee, G.A. Statyukha, P. Biswas, L.T. Angenent, Airborne virus capture and inactivation by an electrostatic particle collector, Environ. Sci. Technol. 43 (2009) 5940–5946.
[39] S.A. Grinshpun, A. Adhikari, C. Li, M. Yermakov, L. Reponen, E. Johansson, M. Trunov, Inactivation of aerosolized viruses in continuous air flow with axial heating, Aerosol Sci. Technol. 44 (2010) 1042–1048.
[40] O.V. Pyankov, E.V. Usachev, O. Pyankova, E. Agranovski, Inactivation of airborne influenza virus by tea tree and eucalyptus oil, Aerosol Sci. Technol. 46 (2012) 1295–1302.
[41] D.G. Duff, A. Baiker, P.P. Edwards, A new hydrosol of gold clusters. 1. Formation and particle size variation, Langmuir 9 (1993) 2301–2309.
[42] K.-S. Chou, C.-Y. Ren, Synthesis of nanosized silver particles by chemical reduction method, Mater. Chem. Phys. 64 (2000) 241–246.
[43] S.-L. Chen, P. Dong, G.-H. Yang, J.-J. Yang, Kinetics of formation of monodisperse colloidal silica particles through the hydrolysis and condensation of tetraethylorthosilicate, Ind. Eng. Chem. Res. 35 (1996) 4487–4493.
[44] D.V. Goia, E. Matijevic, Preparation of monodispersed metal particles, New J. Chem. 11 (1998) 1203–1215.
[45] R.C. Brown, Air Filtration: An Integrated Approach to the Theory and Applications of Fibrous Filters, Pergamon Press, New York, 1993.
[46] U.S. EPA, Chapter 16. Procedures for detecting coliphages, EPA 600/4-84/013, in: Manual of Methods for Virology, U.S. Environmental Protection Agency, Washington, DC, 2001.
[47] W.C. Hinds, Aerosol Technology: Properties, Behavior, and Measurement of Airborne Particles, 2nd ed., John Wiley & Sons, Inc., New York, 1999.
[48] R.C. Brown, W.R. Gray, D.B. Blackford, G.J. Bostock, Effect of industrial aerosols on the performance of electrically charged filter material, Ann. Occup. Hyg. 32 (1988) 271–294.